



# Experimental 2D extended Kalman filter sensor fusion for low-cost GNSS/IMU/Odometers precise positioning system

Adrian Kaczmarek<sup>a,\*</sup>, Witold Rohm<sup>a</sup>, Lasse Klingbeil<sup>b</sup>, Janusz Tchórzewski<sup>c</sup>

<sup>a</sup> Institute of Geodesy and Geoinformatics, Wrocław University of Environmental and Life Sciences, Wrocław, 50375, Poland

<sup>b</sup> Institute of Geodesy and Geoinformation, University of Bonn, Bonn 53115, Germany

<sup>c</sup> StatumGPS sp. z o.o., Wrocław, 50072, Poland

## ARTICLE INFO

### Keywords:

Sensor fusion  
Integration  
Low-cost sensors  
EKF  
GNSS  
RTK  
IMU  
Navigation

## ABSTRACT

The development of satellite techniques and the availability of mobile devices with built-in multi-GNSS (Global Navigation Satellite System) receivers allow the determination of position with increasing accuracy. At the same time, the requirements of users as to the accuracy of positioning are increasing, while the low production costs of the device must be maintained. This paper presents a loosely coupled integration of low-cost sensors (GNSS, IMU (Inertial Measurement Unit), and an odometer) with the use of a nonlinear Kalman filter and a dynamic weight matrix. The integration model was developed for horizontal (2D) components with the simultaneous determination of the azimuth of the test platform. The tests were carried out in the conditions of an open horizon, with partial obscuring of the horizon (passage under an open-work steel structure) and along walls. In this way, the working conditions for an autonomous lawn mower, which are now increasingly used by citizens, were simulated. The position accuracy obtained in these tests is better than 5 cm for horizontal components and better than 1 degrees for the azimuth.

## 1. Introduction and motivation

Currently, there are many different devices that allow the determination of position and orientation (relative or absolute). Modern autonomous devices, that help in everyday life requires cheap and effective tracking solution, ubiquitous GNSS devices that are available in mass-market provide decimeter to even centimeter positioning solution in open horizon setup, however in challenging conditions: partially obscured horizon, signal denied for short time period, multipath [19,35,37], using GNSS receiver only is not sufficient for precise applications in urban and other challenging environments. There are many professional solutions on the market, for precise positioning and orientation, such as mobile mapping systems (e.g., Applanix, Riegl), which include high-end measuring equipment (fiber optic IMU, accelerometers, odometers, professional GNSS antennas and receivers, scanners, photogrammetric cameras, etc.). Thanks to such systems, we can obtain high accuracy, but their price exceeds 50000\$. Stoll & Kutzbach [34] developed an automatic vehicle steering system which using only professional GNSS RTK receiver (the positioning STD achieved from 2.5 to 6.9 cm) and Gan-Mor et al. [9] used GNSS RTK (also professional receiver) to tractor control and obtained centimeter level lateral

accuracy. O'Connor et al. [25] adopted a GNSS RTK system with four antennas to control the tractor and achieved an STD of less than 2.5 cm. Noguchi et al. [24] developed an autonomous robot for agricultural applications using GNSS-RTK and optical IMU (FOG) achieving an RMS of 3 cm, and Takai et al. [36] obtained the accuracy of 5 cm (moving in a straight line and in the open sky horizon).

The above positioning accuracies were obtained under open horizon conditions and without terrain obstructions.

For the average user and mass market applications, commercial and precision solutions are too expensive to incorporate into their devices or systems. In addition to high-end equipment, we can also find low-cost solutions. Low-cost sensors are commercially available for automotive applications, and many manufacturers integrate cheap sensors into their own solutions (vehicles, smartphones, tablets, UAV, etc.).

Such low-cost positioning solutions include, among others, the following: MEMS IMU 3, 6, and 9 DOF (Degrees Of Freedom) sensors, cheap GNSS receivers (L1 or L1/L2), small microcomputers, and classic incremental odometers. The most popular IMU sensors include in their own structures a 3-axis gyroscope and 3-axis accelerometer. Some of the low-cost IMUs [45] also have 3-axis magnetometers. Shin [32] reported that the accuracy of determining the position with the use of low-cost

\* Corresponding author.

E-mail address: [adrian.kaczmarek@upwr.edu.pl](mailto:adrian.kaczmarek@upwr.edu.pl) (A. Kaczmarek).

IMU in case of GPS signal outage could be 10 – 20 m and is similar to what GPS Single Point Positioning (SPP) technique can provide. This positioning accuracy can be maintained for 10 min.

Additionally, just recently mass-market solution list was appended with low-cost, GNSS Real Time Kinematic (RTK) receivers (1–2.5 cm horizontal error) [39]), which can further improve the positioning accuracy. In the paper [26], the authors compare two different positioning strategies SF-DS (Single Frequency - Dual System - L1/B1 GPS + BDS) and DF-SS (Dual Frequency - Single System - L1 / L2 GPS) for RTK positioning using low-cost receivers. It should be added here that according to the manufacturer, the single-frequency receiver used for the tests is used only to determine the precise time (u-blox M8T; T – Timing [40]. The authors proved that low-cost patch antenna receivers for the SF-DS strategy can still provide 100% availability of the instantaneous uncertainty for positioning at the single millimeter level (relative to survey-grade receivers which cost tens of thousands of dollars).

In turn, [22] in their work presents the use of the u-blox NEO-M8P receiver dedicated to RTK positioning. It should be mentioned that the NEO-M8P receiver is a single-frequency receiver for GPS, GLONASS and BeiDou systems, which, according to the manufacturer, guarantees positioning accuracy at the level of single centimeters [38]. The authors showed that a single frequency receiver is perfect for RTK positioning at the centimeter level compared to a high-end receiver, but only in the case of open-sky. Under the conditions of partially obscured horizon, the decrease in accuracy was comparable on both receivers. It should be added that during the positioning tests on the UAV, a cheap GNSS antenna was used, but this also confirmed the high positioning precision in open-sky conditions. For coarse positioning (decimeters) along the trajectory, L1 RTK receivers are sufficient.

In addition to cheap RTK L1 receivers, there are also cheap L1/L2 receivers on the market, such as the u-blox ZED-F9P. In the paper [23], the authors present the use of the ZED-F9P receiver for determining the coordinates using the DF-PPP (Dual-Frequency Precise Point Positioning) strategy. Typically, high-end receivers are used to implement PPP to eliminate ionospheric delay effects. The high price of high-class receivers is an obstacle to precise positioning in common use applications (positioning of city bikes, scooters, etc.). The authors also signal that the effect of ionospheric delay for single-frequency positioning is from decimeters to meters in real time. The applied DF-PPP strategy allowed to obtain the RMS positioning accuracy at the decimeters level (0.27 m, 0.16 m, 0.12 m for the N, E, U components, respectively). In addition, [27] performed positioning and ambiguity estimation tests (BIE - Best Integer Estimation, ILS - Integer Least Squares) of the u-blox ZED-F9P receiver (with dedicated antennas) compared to the Trimble R10 for short and long base double-difference solution ( $\sim 670$  m,  $\sim 112.9$  km). This allowed to determine the positioning accuracy of a low-cost receiver, which is a single centimeter (BIE, ILS). It should be underlined here that the mentioned accuracies were obtained in the post-processing calculations.

All the reported above results in relation to low-cost GNSS receivers confirm that in open horizon in both differential and precise positioning mode low-cost receivers provide centimeter level solution. However, providing consistent coordinates solutions over trajectory with obscured horizon, with potential multipath is a more challenging task. Therefore, we need to combine measurements from several sensors (IMU, GNSS, odometry, LiDAR, camera) using integration algorithm and observation weighting. Moreover, to achieve a positioning accuracy better than 10 cm, we must carefully select sensors in terms of bias and noise.

Literature offers a broad overview of available integration techniques. There is a large body of literature focusing in IMU integration to provide attitude information. One of the challenges in integrating sensor data is stabilizing the gyro drift for all axes. The X and Y axis drift can be eliminated by using the accelerometer [16]. On the other hand, to eliminate the drift and stabilize the Z axis, we can use a magnetometer. However, the magnetometer is very susceptible to external electromagnetic and ferromagnetic interference (electromagnetic

interference from the power supply unit and electric engines in, e.g., a lawnmower, garden steel mesh fences, different steel construction projects, etc.). Of course, we can calibrate the magnetometer, but if we have a variable magnetic field, such calibration will be ineffective or impossible. For this purpose, we can use, for example, the AHRS (Attitude Heading Reference System) method, which joins the 9 DOF of IMU [20,21]. These methodologies allow 1–3 degrees heading accuracy when the sensor is in a static position [18,31].

Another branch of literature is looking into integrating GNSS and other sensor for both positioning and attitude. Zhou et al. [46] present in their work the tightly coupled integration of GNSS (working in SPP mode) and IMU (MEMS) to improve the position accuracy in urban conditions. For this purpose, they use low-cost sensors, and the accuracy of the determined position is about a 3–5 m across whole trajectory with parts of highly obscured satellite view. In turn, [3] show the integration of low-cost sensors GNSS (simulated SPP mode), monocular camera with Simultaneous Localization and Mapping (SLAM) algorithm for precision navigation. The position accuracy obtained by the authors for the horizontal components is better than 1 m. Elisson & Assler [7] presented the integration of GNSS (SPP mode) and INS using among others EKF and Unscented Kalman Filter (UKF) filters. The position accuracy obtained is better than 50 cm. A horizontal position accuracy of better than 15 cm was obtained by [17] by integrating monocular camera, IMU (MEMS) and single frequency multi-GNSS receiver (RTK mode) using tightly coupled EKF fusion. In other approach, [47] integrated GNSS/MEMS-IMU in their work but used from 1 to 4 GNSS receivers. The accuracy of the determined position was from 1.10 m (for one GNSS receiver) to 0.86 m (for four GNSS receivers). In turn (C. [28] performed the GNSS + IMU integration using the low-cost u-blox F9P receiver and low-cost IMU xsens but obtained STD at the level of 0.52, 1.91 and 0.33 m for North, East and Up respectively.

Another algorithm for integrating observations from various sensors was presented by (Abosekeen et al. [1]), and more specifically the RISS (Reduced Inertial Sensor System) algorithm. This system is based on reducing the number of sensors and the observed parameters to a minimum while maintaining the accuracy and reliability of the system. The RISS system uses sensors: GNSS, accelerometer for the X and Y axes, a gyroscope for the Z axis and an odometer. The accelerometer is used to estimate the roll and pitch angles (stable over time), the gyroscope for the azimuth increment, the GNSS, working in absolute positioning mode (SPP solution) and the odometer for the distance measurement. By integrating all these observations, authors are able to obtain 0.5–10 m positioning accuracy (depending on the quality of the GNSS receiver and IMU) in virtually all terrain conditions. The advantage of RISS is also a small number of sensors, which translates into the cost of the entire system and the computing power needed for sensor fusion. Unfortunately, RISS also has disadvantages - it is susceptible to cumulative azimuth drift over time, and thus also increases the position error. The RISS positioning accuracy is 0.5–10 m, depending on the calculation strategy used (for example: adding heading drift compensation). The stabilization of the heading drift is possible thanks to the use of a magnetometer, which translates into accuracy of 99 m (for RISS/GPS) and 12 m (for Mag/RISS/GPS) [1]. The use of RISS in PPP allows for positioning accuracy better than 50 cm [8] which can be successfully used in navigating a car in a lane.

Classical integration algorithm is the well-known Kalman filter in a linear (KF-Kalman Filter) or nonlinear (EKF-Extended Kalman Filter) version [33]. Research shows that the accuracy of GNSS-IMU sensor integration using Kalman Filter depends on the approach used (loosely, tightly, or deeply coupling), proper filtering setup [43], and the use of additional sensors such as multi-antennas, odometry, cameras, and scanners [6,30]. Some of these approaches allow the accurate determination of the relative position when there is interference or no GNSS signal [4,5,41,42]. The use of data integration from different sensors can support standalone GNSS positioning. Commercial solutions combine the data to eliminate the impact of inertial navigation errors (gyroscope

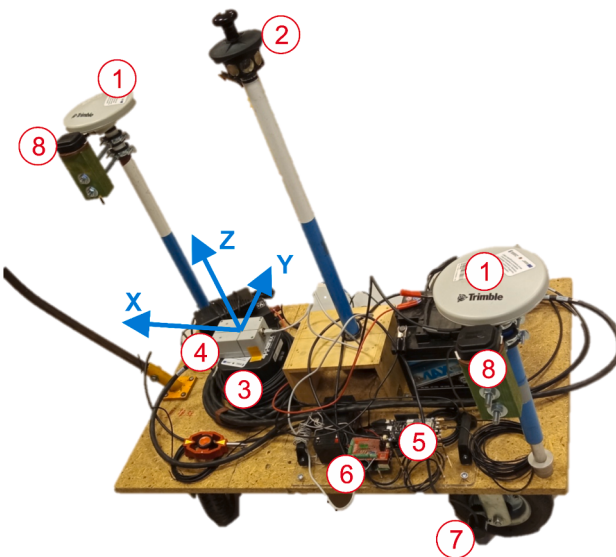


**Fig. 1.** Test platform with marked coordinate system.

drift) and provide them with greater reliability compared to the stand-alone GNSS solution. Detailed methods for the implementation of tightly and loosely coupled filtration were presented by [2,10,29].

The motivation to undertake this research is to develop a cheap system (under 1500\$) for precise positioning in all terrain conditions, while maintaining positioning accuracy better than 5 cm. Such a system will solve the problems of accurate positioning where the RTK GNSS fix positioning is lost. Our system could be used in agricultural machines or similar devices of common use, such as an autonomous mower. Many vehicle positioning solutions are based only on the GNSS receiver. For example, [12] used GNSS RTK L1 (low-cost receiver) for autonomous system (speed sprayer) and got RMS error of centimeters level. In addition, they noted that the positioning accuracy is not repeatable and reliable. In case of signal interference. [44] in his research presented the integration of GNSS + IMU for an automatic rice planter but used professional integration system. The accuracies they got in the open horizon are better than 10 cm for the lateral position and the azimuth accuracy is 5 degrees. It should be added here that the obtained accuracies are for a rectilinear trajectory.

High positioning accuracy in all environmental conditions is required in autonomous vehicles that are commonly used (e.g., lawn mowers, which will move without a cable limiting the operating area - working boundary with a magnetic loop). In addition, such a system could be used to navigate autonomous warehouse trucks around the production halls. In addition, the minimum number of sensors used will translate into a low-cost of the system and low computational complexity. The system presented in the paper estimates the horizontal components and the azimuth, maintaining the assumed accuracy better than 5 cm in all tested environmental conditions. For autonomous cars traveling on the road (keeping the trajectory) a positioning accuracy of about 0.5 m is sufficient. However, for devices such as a lawn mower, this accuracy must be within a 5-centimeter margin. The research that was carried out in this paper focuses on the integration of low-cost GNSS, low-cost IMU (1 DOF z-axis), and low-cost odometer (optical encoder) sensors to obtain a precise horizontal position. To obtain a precise and stable orientation, the special properties of two sensors were used: the azimuth from two GNSS antennas (long-term stability, but not very precise) and orientation from the IMU (short-term stability, but with high precision). A synchronous Extended Kalman Filter was used for integration, combining the heading and position into one calculating process. In the integration algorithm, we also use dynamic weighting of GNSS observations, which is dependent on signal disturbances. The dynamic weighting of observations is an innovation in our EKF filter,

**Table 1**

The hardware content of the test platform.

No.	Name	No.	Name
1	Applanix GNSS antennas	5	u-blox GNSS RTK receivers
2	Geodetic 360° prism	6	Microcomputer
3	Applanix IMU (fiber optic)	7	Odometers (optical)
4	Low-cost MEMS IMU	8	u-blox antennas

**Table 2**

Data collected by the test platform.

Sensor name	Type of data	Data unit	Rate in Hz
GNSS receiver (u-blox F9P)	RTK horizontal position	[m]	5
IMU (xsens MTi-7)	Only z-axis (angular rate)	[rad/s]	50
Odometer	Distance increment	[m]	50
Applanix - position	Horizontal position	[m]	200
Applanix - azimuth (only reference data)	azimuth	[deg]	200
Total station (only reference data)	Horizontal position	[m]	1

moreover we limit the number of sensors, finally our solution is built only with low-cost components not exceeding the 1500\$ price tag for all components. Thanks to this, we significantly increase the positioning accuracy in all tested conditions (not only in the open horizon and along a rectilinear trajectory).

The paper has the following structure: section 1 contains the introduction, the Input data description follows in section 2, and the methodology, results, discussed and conclusions in sections 3, 4, 5 and 6, respectively.

## 2. Input data

A test platform (Fig. 1) has been developed for data collection. This

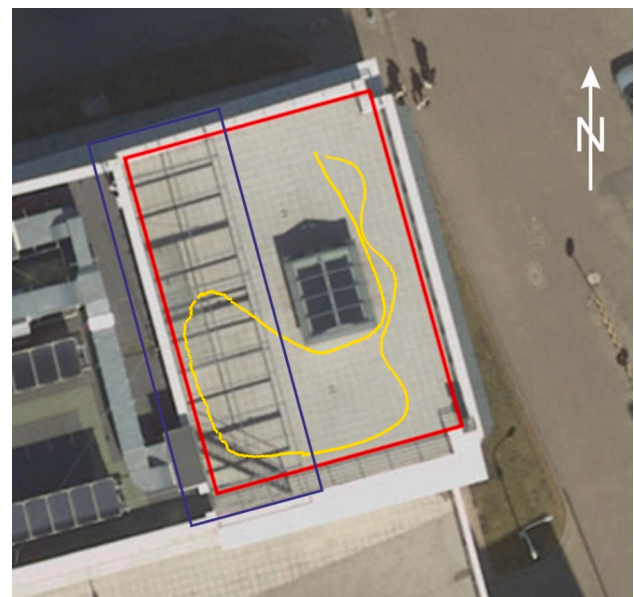


**Fig. 2.** Test area - Wroclaw University of Environmental and Life Sciences (Poland) - terrace of one of the University buildings (with raw u-blox GNSS trajectory - yellow). The blue line represents the horizon occult area on the west side where we have only FLOAT solution. (For interpretation of the references to colour in this figure legend, the reader is referred to the web version of this article.)

platform included low-cost sensors (u-blox GNSS RTK F9P, xsens IMU MTi-7, odometer-optical encoder mounted on two wheels, and a microcomputer Raspberry Pi to collect data from the low-cost sensors). Additionally, the test platform also includes high-end equipment for professional mobile navigation (Applanix POS LV 120 V5), which provides a high rate and an accurate reference azimuth and position. A geodetic 360 degrees prism was also installed for an independent position reference. The geodetic reference position was measured using the robotic total station (Trimble S8). The positions of Applanix and the total station were used as references for sensor fusion. The platform coordinate system was hooked in the center of the Applanix/xsens IMU, where the X axis was directed along the direction of travel and the Y axis was directed transversely to the right and Z axis to the Up. [Table 2](#) shows the data that was collected by the test platform. Related to [Table 2](#), Applanix reference data were calculated using POSPac MMS software, which uses a tightly coupled integration filter of data from a fiber optic IMU (6 DOF) and two GNSS antennas. The GNSS antennas will determine the absolute azimuth and position, while the IMU presents the precise orientation angles. Integration is performed in post-processing in POSPac MMS software. Apart from the raw sensor data, we need to add information about precise GNSS orbits, data from the reference station to solve RTK solution models of the receiver, and an antenna calibration file. As a result, we get a very accurate and stable position and orientation solution. [Table 1](#) shows the description of the equipment of the test platform.

The test area was located on the terrace of Wrocław University of Environmental and Life Sciences (UPWr) university building ([Fig. 2](#)) at a height of about 20 m above ground level. On this terrace, there were conditions for taking measurements in the open horizon (on the right on [Fig. 2](#)), and it was possible to simulate the obstacles of the horizon for GNSS measurements (passages near the wall and under a metal open-work structure provide the deterioration of the accuracy of the GNSS position - on the left in [Fig. 2](#)). Data were collected on a test platform moving with a speed of about 20 cm/s thereby simulating the constant speed motion of the lawn mower. The effect of velocity of the platform on data collection has not been investigated, as a constant speed of movement of this type of devices has been assumed.

### 3. Methodology

In our research, we used a modified loosely coupled strategy (sensor fusion) based on an Extended Kalman Filter (EKF) with standard polar equations to determine the geodetic position. The strategy used some of the measured observations (IMU z-axis angular rate and distance from odometry) as control inputs that were not modeled in the filter. The use of a loosely coupled integration strategy allows the minimization of the complexity of the algorithm and keeps the hardware solution to a minimum while maintaining the high accuracy of the final position. Low-cost GNSS receivers provide raw observations and antenna calibration models to be able to apply a tightly coupled strategy but we didn't use it in our strategy. In addition, the position determined by the test platform must be in real time, so this is another argument in favor of using a loosely coupled filter (some of the data required by a tightly coupled filter, might not meet high precision demand such as predicted orbits or satellite clocks). In our filter we used the RTK position directly given from u-blox in relation to the WROC base station, which provided RTK corrections using NTRIP (the exact processing strategy of the RTK u-blox FIX/FLOAT solution is not known). Moreover, it is not known how u-blox F9P determines ambiguities: whether it solves them for all systems simultaneously or separately for each of the satellites, eg GPS. The baseline between the base and the rover was about 60 m. As a result, we could neglect the ionospheric and tropospheric delays in our calculations. The discussed application concept assumes that devices

developed in this study will be used with short baseline between the base and the rover (e.g., in cities for a fleet of mowers). On the equation [\(1\)](#) and [\(2\)](#) we show the classic RTK solution method for a single base reference station whereby users can obtain centimeter level position accuracy in real time [\[15\]](#).

$$\lambda^s \phi_A^S(t_0) = \varrho_A^S(t_0) + \Delta \varrho_A^S(t_0) + \Delta \varrho^S(t_0) + \Delta \varrho_A(t_0) + \lambda^S N_A^S \quad (1)$$

where:  $\varrho_A^S(t_0)$  is the geometric range,  $\Delta \varrho_A^S(t_0)$  is the satellite – receiver dependent bias,  $\Delta \varrho^S(t_0)$  is the satellite dependent only,  $\Delta \varrho_A(t_0)$  is the receiver dependent only and  $N_A^S$  is the phase ambiguity.

$$\lambda^s \phi_A^S(t_0)_{corrected} = \varrho_A^S(t) + \Delta \varrho_{AB}(t) + \lambda^S N_{AB}^S \quad (2)$$

Equation [\(2\)](#) shows results for corrected phase ranges where  $\Delta \varrho_{AB}(t) = \Delta \varrho_B(t) - \Delta \varrho_A(t)$  and  $N_{AB}^S = N_B^S - N_A^S$  is the difference of phase ambiguities. The position at the rover in site B is performed with corrected pseudorange phase [\[14\]](#).

The use of a loosely coupled filter and use of position coordinates directly from the receiver also does not require high computing power. Thanks to this, we can use low-cost computers such as Arduino or Raspberry Pi for autonomous vehicle navigation. However, this study is simulated real-time solution, i.e., the recorded real-time observations were integrated in post-processing mode.

#### 3.1. Extended Kalman filter implementation

The EKF filter implements data processing from the following sensors: GNSS RTK, IMU (Z-axis) and odometer. Based on these observations data, were calculated the azimuth angle increment which was calculated from the gyroscope Z-axis, and the coordinate increment (X and Y) based on the azimuth and odometer distance. These data were used as a control input in the prediction step (eq. [\(3\)](#), [4](#), [5](#)). Additionally, system noise for these sensors was added to the filter. In the update step, the apart Kalman gain [\(8\)](#), position, heading, and covariance matrix correction [\(10\)](#) were included R matrix [\(12\)](#), which has a constant or dynamic status (values - weighting in the matrix depend on the type of GNSS fix, float, or navigation solution from u-blox flags). This methodology (equations [\(3\)](#) – [\(12\)](#)) is based on a modified version of [\[11\]](#). The prediction steps include equations [\(3\)](#) – [\(7\)](#) and the correction steps include equations [\(8\)](#) – [\(12\)](#). Correction step included data from GNSS receivers (horizontal coordinates and azimuth calculated from two GNSS antennas). However, the data from the gyroscope and odometer were used only for position prediction. Filter was updated every 0.2 s (u-blox sample rate was equal 5 Hz). The filter structure assumes a minimum number of sensors and work in flat areas. Therefore, the roll and pitch angles and the height coordinate are not estimated.

$$x_k^- = f(x_{k-1}, u_k, w_k) = \begin{bmatrix} x_k \\ y_k \\ \varphi_k \end{bmatrix} = \begin{bmatrix} x_{k-1} + \cos(\varphi_{k-1}) \cdot (\Delta odo_k + w_{odo}) \\ y_{k-1} + \sin(\varphi_{k-1}) \cdot (\Delta odo_k + w_{odo}) \\ \varphi_{k-1} + (\omega_{gyro,k} + w_{gyro}) \cdot \Delta t \end{bmatrix} \quad (3)$$

$$P_k^- = \Phi P_{k-1} \Phi^T + G Q G^T \quad (4)$$

$$\Phi_{k-1} = \frac{\partial f(x, u, w)}{\partial x} = \begin{bmatrix} 1 & 0 & -\sin(\varphi_{k-1}) \cdot \Delta odo_k \\ 0 & 1 & \cos(\varphi_{k-1}) \cdot \Delta odo_k \\ 0 & 0 & 1 \end{bmatrix}_{x=x_{k-1}, u=u_{k-1}} \quad (5)$$

$$Q = \begin{bmatrix} \sigma_{odo}^2 & 0 \\ 0 & \sigma_{gyro}^2 \end{bmatrix} \quad (6)$$

$$G = \frac{\partial f(x, u, w)}{\partial w} = \begin{bmatrix} \cos(\varphi_{k-1}) & 0 \\ \sin(\varphi_{k-1}) & 0 \\ 0 & \Delta t \end{bmatrix}_{x=x_{k-1}, u=u_{k-1}} \quad (7)$$

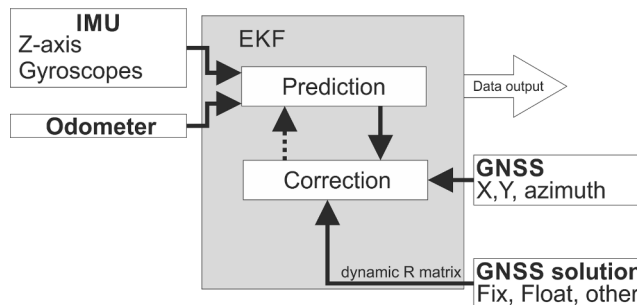


**Fig. 3.** Block diagram of the operating principle of EKF integration with dynamic weighing (R matrix).

$$K_k = P_k^- H^T (H P_k^- H^T + R)^{-1} \quad (8)$$

$$x_k = x_k^- + K_k (z_k - h(x_k^-)) \quad (9)$$

$$P_k = (I - K_k H) P_k^- \quad (10)$$

Measurement Vector:

$$z_k = \begin{bmatrix} x_{GPS,k} \\ y_{GPS,k} \\ \varphi_{GPS,k} \end{bmatrix} \quad (11)$$

Measurement Noise:

$$R = \begin{bmatrix} \sigma_{GPS,X}^2 & 0 & 0 \\ 0 & \sigma_{GPS,Y}^2 & 0 \\ 0 & 0 & \sigma_{GPS,\varphi}^2 \end{bmatrix} \quad (12)$$

where:

$\Delta odo_k, \omega_{gyro,k}$  - control input values (angular rate, odometry distance),  $w_{odo}, w_{gyro}$  - noise of control input,  $R$  - measurement noise (position and heading),  $Q$  - control input noise matrix,  $G$  - system noise of control inputs. Fig. 3 shows the general principle of our filter with dynamic weighting.

Weighting values for all sensors have been assigned from technical notes and modified during filter tuning.

### 3.2. Solution validation

Validation of the accuracy of the position determined using Applanix

**Table 3**

The stages of an experimental project.

Stage	Description
Determination of position accuracy from Applanix solution	Calculation of RMS values between the position of the total station (reference trajectory for Applanix) and the solution from Applanix POSPac software (RTK position is computed from raw observations with using precise orbits. Then the IMU integration is performed, and finally the trajectory is smoothed with the SBET process). DMI was disabled.
Determination of position accuracy from u-blox solution	Calculation of RMS values between the position from u-blox and the solution from Applanix(reference trajectory for u-blox and EKF)
The first variant of EKF filter tuning	Assumption: $\Delta t = 0.02$ s; $R$ matrix = constant; $Q$ matrix = constant
The second variant of EKF filter tuning	Assumption: $\Delta t = 0.02$ s; $R$ matrix = dynamic (value depends on GNSS RTK solution); $Q$ matrix = constant
The third variant of EKF filter tuning	Assumption: $\Delta t = 0.02$ s + offset; $R$ and $Q$ matrices are the same as in the second variant
The fourth variant of EKF filter tuning	Assumption: $\Delta t = 0.02$ s + offset; $\Delta t$ and $R$ matrices are the same as in the third variant; Added additional noise to odometer in $Q$ matrix

**Table 4**  
Position accuracy of Applanix mobile mapping system.

Direction	Applanix position accuracy [RMS]
North	0.014 m
East	0.013 m
Heading	0.1 degree (value after post-processing in POSPac software)

was compared to the position determined by the total station. The position of the total station and Applanix had the same timestamp. It should be added here that the Applanix position was determined with a frequency of 200 Hz, while the position from the total station was 1 Hz. Thanks to the timestamp, it was possible to select identical points for Applanix and the total station and calculate RMS values (13). The RMS values for the comparisons were determined in the same way for Applanix – u-blox and Applanix-EKF using the following formula (13).

$$RMS = \sqrt{\frac{\sum_{i=1}^n (pos_{EKF/ublox_i} - ref_i)^2}{n-1}} \quad (13)$$

where

$pos_{EKF/ublox}$  - position from EKF filter or u-blox receiver,  $ref$  - reference position from Applanix or total station.

### 3.3. Experimental design

The experimental design consisted of the steps of determining the accuracy of the reference trajectory and tuning the integration filter. The main stages of the experiment are included in Table 3.

RMS values after each variant were calculated in the same way as for the reference trajectory according to formula (13). Details of the individual steps (variants) are described in the Results section.

## 4. Results

### 4.1. Accuracy of the reference position

Before starting the actual analyses, it was necessary to determine the positioning accuracy of the Applanix equipment. To compare the accuracy of determining the position, an independent reference from tachimetry was used. In Table 4 we can see the Applanix horizontal position accuracy referenced to the tachimetry, and we can see that the accuracy is about 1.5 cm for the horizontal component. The azimuth

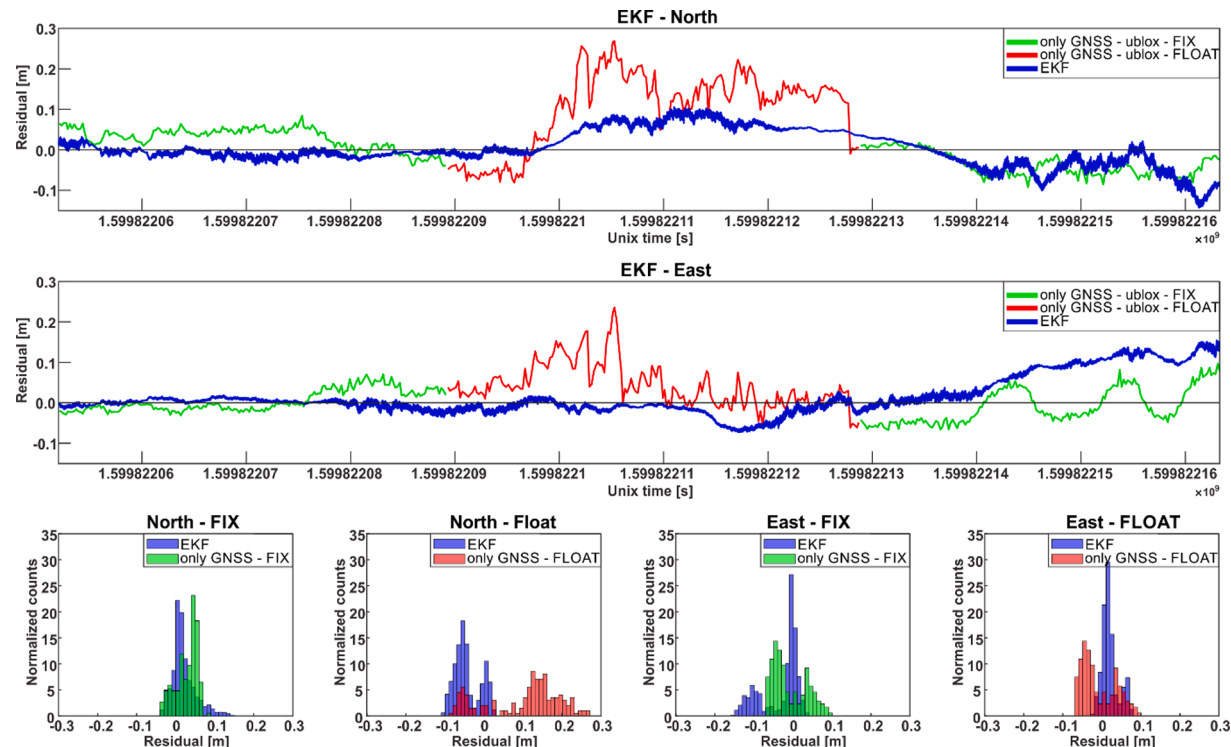


**Fig. 4.** U-blox F9P receiver and EKF sensors fusion (first variant) position residuals.

**Table 5**

U-blox F9P receiver horizontal and EKF sensors fusion (first variant) position accuracy (RMS values in meters [m]).

Direction	North (FIX)	North (FLOAT)	East (FIX)	East (FLOAT)
u-blox	0.043	0.138	0.041	0.068
EKF	0.036	0.054	0.058	0.028

accuracy is equal to 0.1 degrees. Results from the Applanix mobile mapping system were used for further analysis because this data is denser than tachimetry (200 Hz and 1 Hz, respectively).

#### 4.2. Positioning accuracy using only the low-cost GNSS RTK receiver and first variant of EKF sensor fusion

The low-cost RTK L1/L2 receivers determined the coordinates relative to the WROC reference station (Wrocław, Poland), which was located approximately 60 m from the test area. The corrections to the receivers were transmitted via the GSM network with the NTRIP protocol (a single reference station was used). The Fig. 4 shows the u-blox F9P position residuals referenced to the Applanix solution (divided into FIX (green) and FLOAT (red) solution).

From Fig. 4 and Table 5, we can see that that already at this stage, the position of the low-cost receiver is not precise, and its accuracy is above 10 cm for East direction and the residuals exceeds 20 cm for North and East direction. The reason for such high residues is the loss of the FIX

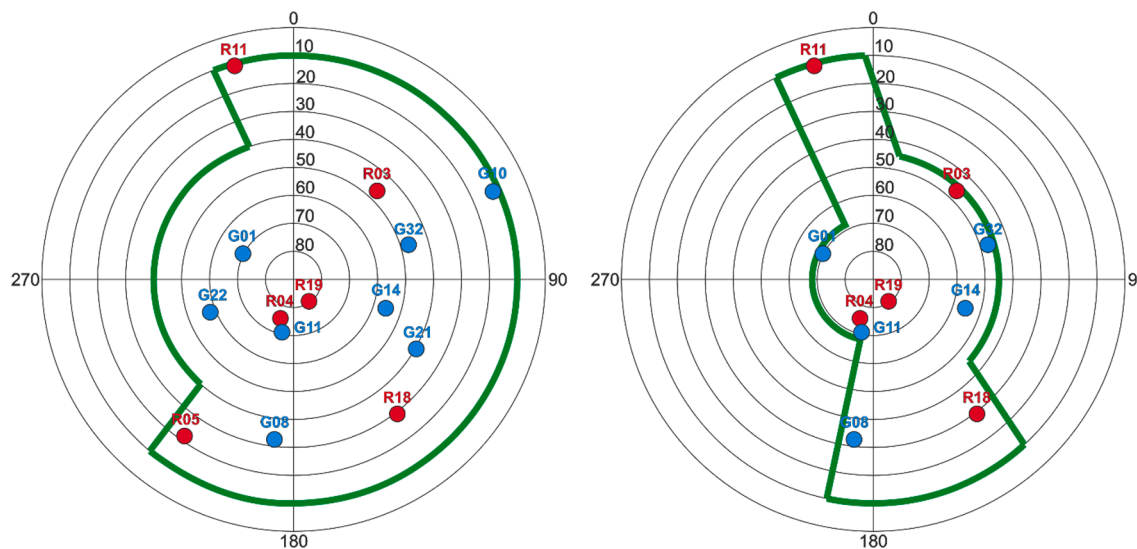


**Fig. 5.** Distribution of satellites during tests (from the left: FIX solution; FLOAT solution).

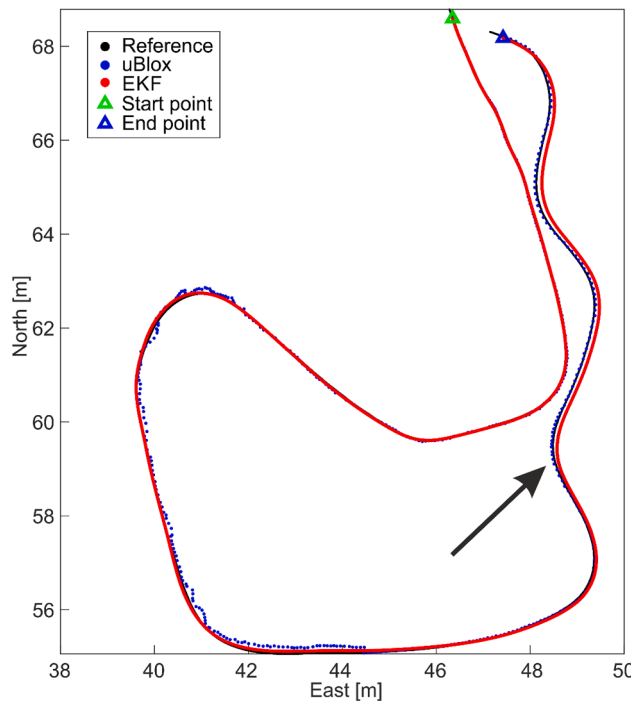


**Fig. 6.** Accuracy position estimation after sensor fusion. The black arrow shows starts a problem with time synchronization between sensors (cumulative drift of Raspberry Pi Real-Time Clock (RTC)).

solution (when driving close to the wall) and covering the horizon, which are shown in Fig. 5. The elevation mask was set to 10 degrees for u-blox receivers.

The first integration variant consisted of assuming constant optimistic values in the R and Q matrices, and the time interval was 0.02 s. The results were presented in Fig. 6 and residuals in Fig. 4. In Figs. 4 and

6, we can see that there is an improvement in determining the position accuracy where we had a float solution. On the other hand, there is a deterioration in the accuracy of the determined position in the place where the measurement platform was driving the slalom (Fig. 6). This situation we also can see in residuals in Fig. 4 for sensor fusion (East component). This is probably due to the starting problem with time synchronization between sensors. For the FLOAT solution for the North and East components, we have achieved a twofold increase in the accuracy of the determined position (Table 5). In the histograms in Fig. 4, we also see an improvement in the residual distribution compared to the solution only from u-blox GNSS.

#### 4.3. Positioning accuracy after EKF sensor fusion - second variant

The second variant of filter tuning was to change the matrix R from constant to dynamic. In this version of the filter, the type of GNSS solution (fix, float, or navigation) was checked and depending on the type of solution, one of the three R matrices was selected. Checking the GNSS solution condition consists of the use of the classical if loop. The results are shown in Fig. 7 and Table 6. In Fig. 7, we also see a deterioration in position accuracy but only for FLOAT solution compared to the EKF first variant. It is probably caused by a change in EKF weighting and a problem with time synchronization between sensors.

#### 4.4. Positioning accuracy after EKF sensor fusion - third variant

The third variant of the filter consisted of the empirical selection of the correction of the time synchronization between the sensors (time

**Table 6**

U-blox F9P receiver horizontal and EKF sensors fusion (second variant) position accuracy (RMS values in meters [m]).

Direction	North (FIX)	North (FLOAT)	East (FIX)	East (FLOAT)
u-blox	0.043	0.138	0.041	0.068
EKF	0.046	0.032	0.046	0.074

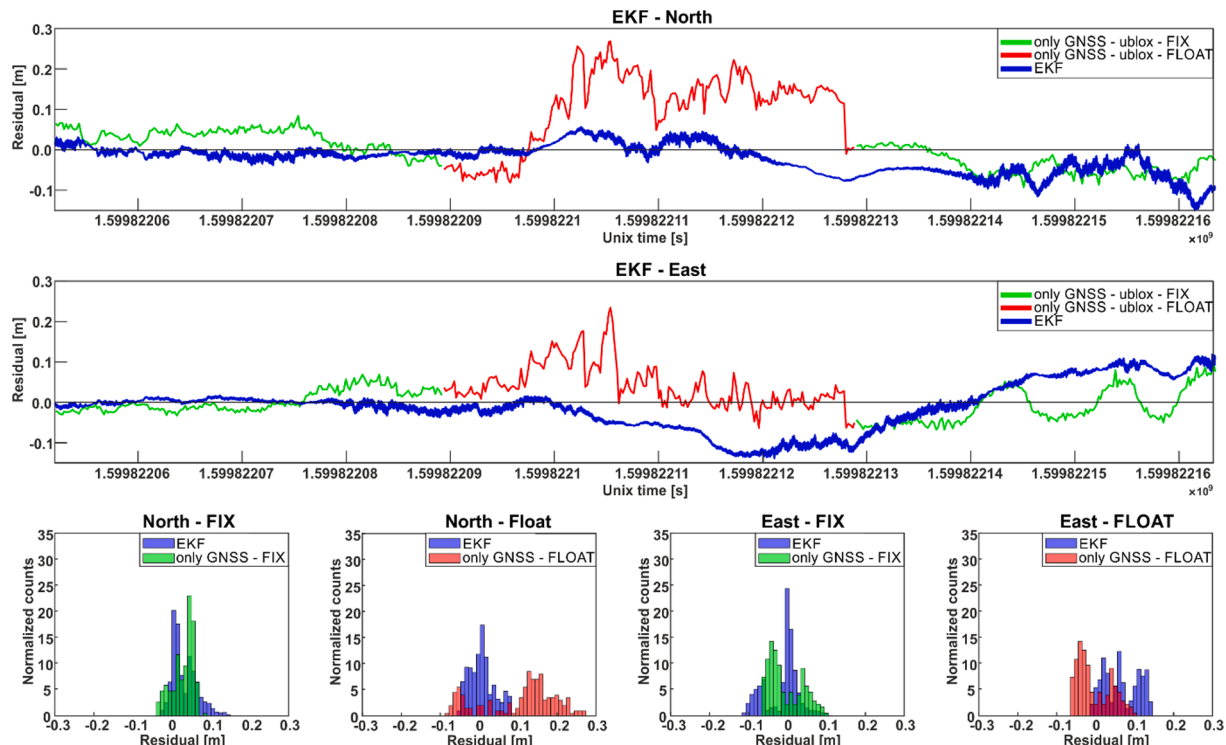


**Fig. 7.** U-blox F9P receiver and EKF sensors fusion (second variant) position residuals.

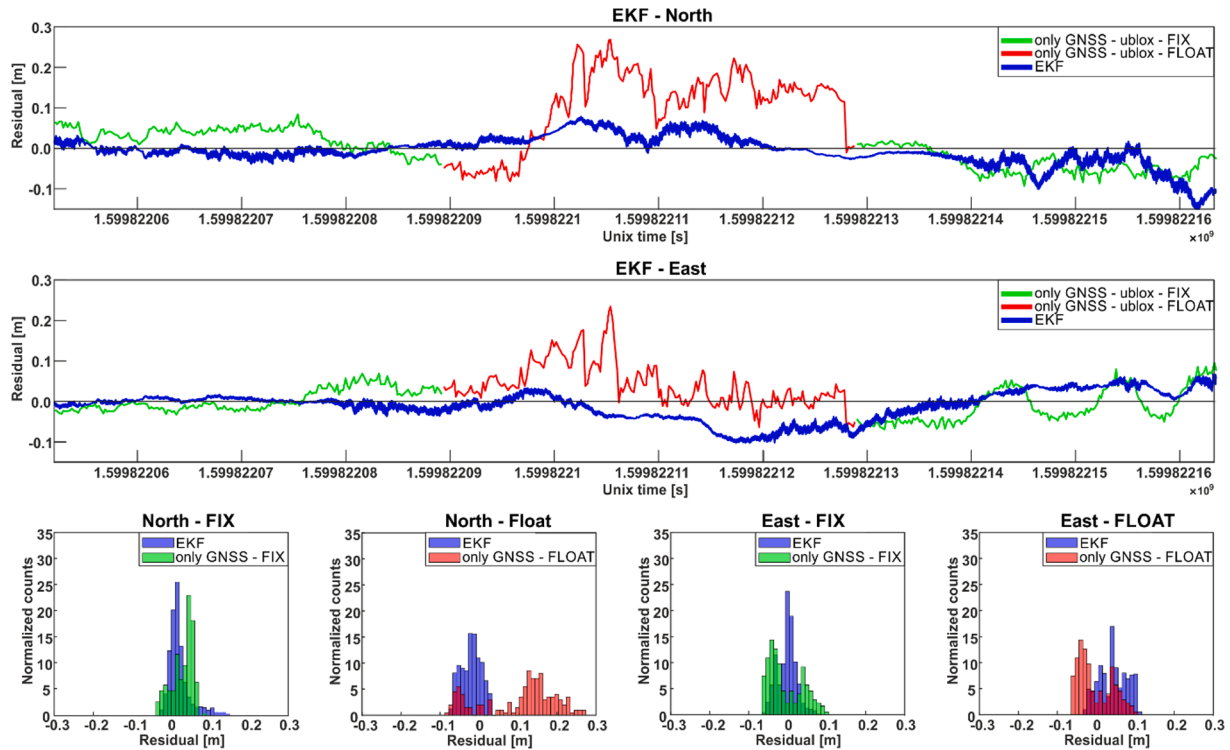


**Fig. 8.** U-blox F9P receiver and EKF sensors fusion (third variant) position residuals.

**Table 7**  
U-blox F9P receiver horizontal and EKF sensors fusion (third variant) position accuracy (RMS values in meters [m]).

Direction	North (FIX)	North (FLOAT)	East (FIX)	East (FLOAT)
u-blox	0.043	0.138	0.041	0.068
EKF	0.037	0.034	0.024	0.051

interval = 0.02 s + 75  $\mu$ s). The Q and R matrices are the same as in the second variant. Increasing the sampling interval significantly improved the quality of the estimated position. The results can be seen in Fig. 8 and Table 7. It should be noted here that precise time synchronization between sensors is essential if we want to use the synchronous Extended Kalman Filter.

#### 4.5. Positioning accuracy after EKF sensor fusion - fourth variant

In the fourth variant of the filter, the noise value in the Q matrix for the odometer was modified (the R matrix and the time interval remained the same as in the third variant). The change in the noise value is due to the fact that the wheel circumference may not be accurately determined or may have changed over time (tire rubbing, insufficient tire pressure, etc.). For this purpose, 0.3 mm was added to the original noise value, which was selected empirically. The result of these changes is presented in Fig. 9 and Table 8. In the last variant, we can see that improving the time interval, adding dynamic weighting, and changing the noise of the distance measurement ultimately contribute to the high quality of the measurement platform's position estimation. We also see that the residuals are smaller than for the other variants and relative to the GNSS receiver itself. In addition, EKF integration improved the accuracy of the solution in places where FIX occurred to 1.9 cm for horizontal components in relation to the GNSS solution.

#### 4.6. Azimuth (heading) accuracy after EKF sensor fusion

Fig. 10 shows the results of azimuth estimation based on the filter

parameters of the fourth variant. In contrast, Fig. 11 shows the combination of short-term (high accuracy) and long-term (low accuracy) directional stability (for IMU and GNSS, respectively). In Table 9, we can see that the azimuth accuracy is almost ten times better than the azimuth of GNSS receivers.

## 5. Discussion

GNSS positioning and attitude determination is currently an intensively research area, and definitely a large leap forward has been achieved in the current solutions. Starting with [32], findings of being able to achieve consistent 10 – 20 m in all terrain conditions using GPS standard positioning service and basic IMU sensors, and just recently published findings by [17] that achieved 0.15 m accuracy using RTK GNSS solution and IMU sensor. This large increase of quality in positioning must be attributed to the use of RTK [26] or PPP [23] algorithms mass-market single and double frequency phase receivers such as NEO-M8P [22], NEO-M8T [26], ZED-F9P [23,27], these receivers will attain consistent positioning solution on the level of 10 cm or better in open sky conditions.

However, as shown in number of other studies, the solution quickly deteriorates in challenging environmental conditions e.g., in [17] from 0.15 m to 2 m, for RTK precise solution, or from 8 m to 20 m for standard point positioning [46]. Use of other observations such as gyroscope, accelerometer, odometer is therefore indispensable. Algorithm that is widely adopted in the literature and also used in this study is EKF [33]. The solution demonstrated in this research uses ZED-F9P receiver that produces high-quality, solution in the open sky horizon and fixed solution (see green line on Figs. 4, 7, 8, 9), which is similar to the work done by [26]. However, sensors integration that has impact on the float section of the solution (see red line on Figs. 4, 7, 8, 9), and the iterative approach (see Table 3) to attain high consistency between reference positioning and investigated device, was relatively seldom reported in the literature. Table 5–8 show the RMS values for each filter tuning step. It should be added here that these are the values for individual components (FIX and FLOAT), which show the operation of the integration

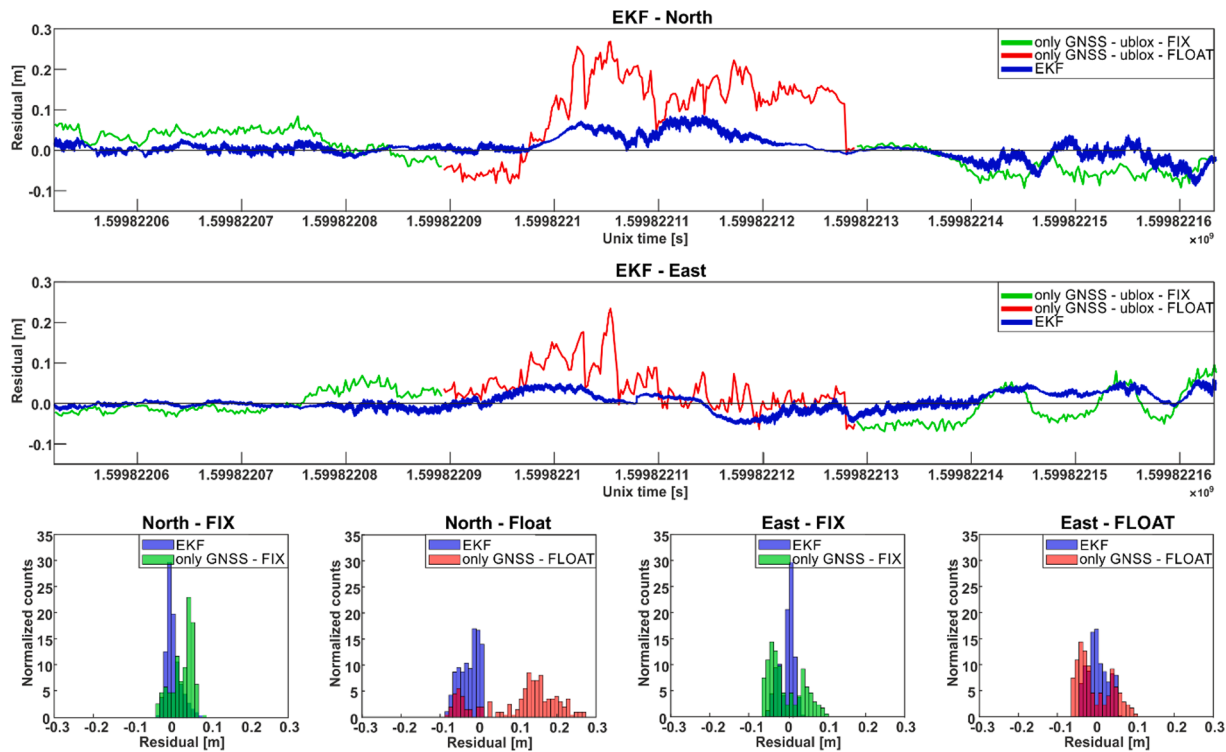


**Fig. 9.** U-blox F9P receiver and EKF sensors fusion (fourth variant) position residuals.

**Table 8**  
Horizontal position accuracy after sensor fusion - fourth variant.

Direction	North (FIX)	North (FLOAT)	East (FIX)	East (FLOAT)
u-blox	0.043	0.138	0.041	0.068
EKF	0.019	0.037	0.019	0.026

in places where the GNSS signal deteriorates (horizon shading with a high elevation mask - above 70 degrees East-West). Adaptive, changes in the R matrices (12) and subsequently improving stochastic part of the solution with Q matrix (6), allowed to improve positioning to solution better than 5 cm. It also helped to identify major problems persistent in the system: 1) synchronization time, in many studies Positioning Pulse Signal is used to synchronize all the data, in this study only internal clock was used to assessing time stamp, 2) wheels shape inaccuracies.

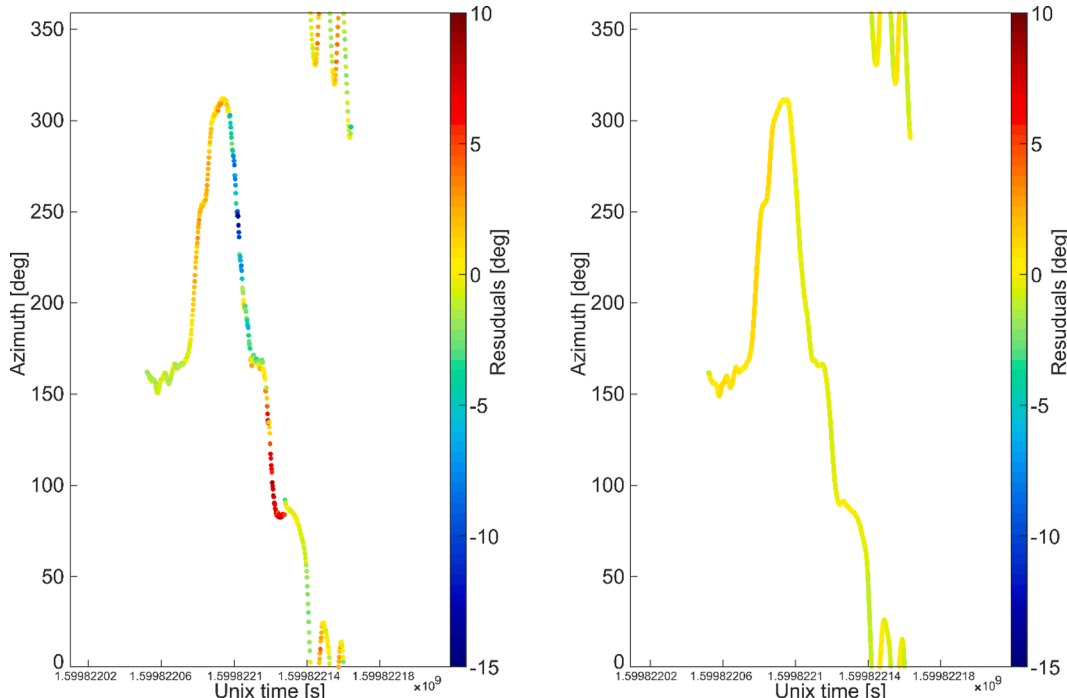


**Fig. 10.** Azimuth residuals before (left - u-blox azimuth) and after (right) sensor fusion - unit: degrees.

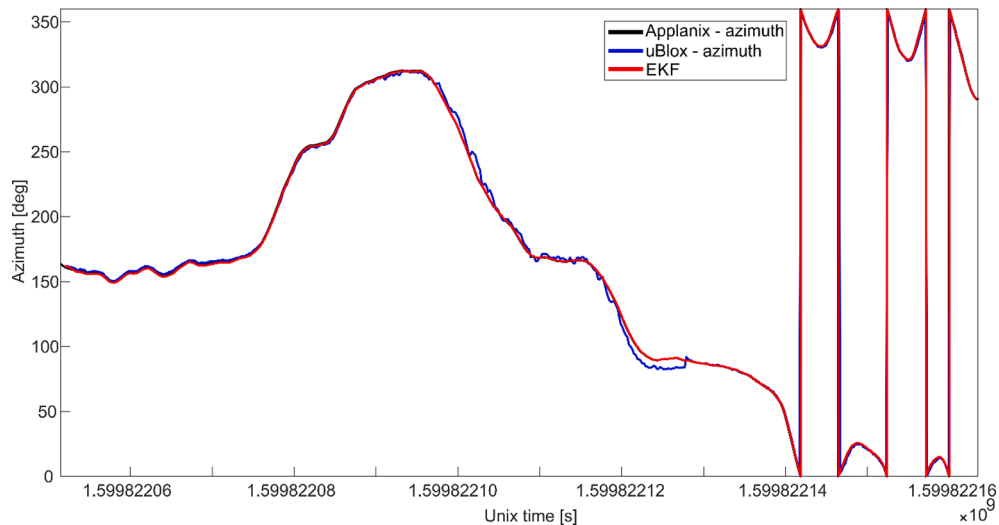


**Fig. 11.** GNSS azimuth and IMU sensor fusion results (blue - GNSS azimuth, red - sensor fusion). (For interpretation of the references to colour in this figure legend, the reader is referred to the web version of this article.)

**Table 9**  
Azimuth accuracy after sensor fusion (EKF).

Heading	Heading accuracy [RMS]
GNSS (u-blox)	5.55 degrees
EKF	0.59 degrees

**Table 10**  
Summary of literature reporting positioning of moving devices with GNSS only device or a positioning system, based on professional or low-cost sensors.

Reference	Type of sensors (professional = Y; low- cost = L)	Environmental conditions	Horizontal Error [m]
[25]	4-antennas GPS system (Y)	Open horizon	$\leq 0.25$ m
[24]	GNSS RTK (Y) + IMU (FOG) (Y)	Open horizon	0.03 m
[34]	GNSS RTK (Y)	Open horizon	0.25 – 0.69 m
[32]	GPS (L) + IMU(L)	Open horizon	10–20 m
[9]	GNSS RTK (Y)	Open horizon	Centimeter level
[36]	GNSS RTK (Y) + IMU MEMS (L)	Open horizon	0.05 m
[7]	GNSS (SPP mode) (L) + IMU(L)	Open Horizon	0.50 m
[46]	GNSS (SPP mode) (L) + IMU MEMS (L)	Open Horizon	3–5 m
[44]	GNSS RTK + IMU	Open horizon	$\leq 0.10$ m
[3]	GNSS (SPP mode)(L) + SLAM	Open horizon/ obscuring the horizon	$\leq 1$ m
[17]	GNSS RTK L1 + camera + IMU(L)	Open horizon/ obscuring the horizon	0.15 m
[1]	GNSS (SPP mode)(L) + IMU (L) + odometry (L)	Open horizon/ obscuring the horizon	0.50–10 m
[13]	GNSS RTK L1 (L)	Open horizon	Centimeter level
[28]	GNSS RTK (L) + IMU (L)	Open horizon	50 – 190 cm
Our solution	GNSS RTK (L) + IMU (L) + odometer (L)	Different environmental condition	$\leq 0.05$ m

The proposed solution has however several limitations: 1) loosely coupled Kalman Filter, will break in case of complete blocking horizon for longer than several seconds as the azimuth and position observations provided to the EKF (11) are provided by GNSS, 2) dropping pitch and roll angle in the estimation algorithm does not allow to use the system

effectively in the rough terrain, 3) further development is required to implement obtained solution in the microcomputer such as Raspberry-Pi and to test feasibility of such approach in terms of available computing power.

The Table 10 is a demonstration of the reported in literature results. We can see that low-cost solutions can compete with professional devices and integrating solutions. In Table 10 we can see that the obtained positioning accuracies mostly concern the open horizon and with the use of professional sensors. Accuracies range (for professional and low-cost sensors) from a centimeter level [9] to about 20 m [32]. Our system was able to achieve an accuracy of better than 5 cm in all environmental conditions and was made of only low-cost sensors.

## 6. Conclusion

The integration of low-cost sensors allowed us to obtain a very high accuracy of the estimated position. The obtained final values (for the FLOAT solution) are four - and two times better than before the integration (13.8 cm vs 3.7 cm for the North component and 6.8 cm vs 2.6 cm for the EAST component). Moreover, the accuracy for the trajectory with the FIX solution for both horizontal components has doubled from 4.3 cm to 1.9 cm. Moreover, the combination of the short- and long-term stability of the GNSS and IMU sensors allowed us to obtain a precise azimuth, the accuracy of which was 0.59 degrees (Table 9).

It can be noted that the use of some of the observations (odometer and IMU) as control observations gave satisfactory results, allowing us to run positioning with a sub-decimeter accuracy comparable to high-end solutions (e.g. Applanix). At this point, it should be added that in next step the time synchronization between the sensors is essential. A lack of time synchronization on the level of 1  $\mu$ s causes fluctuations in the estimated position. To improve the accuracy of time synchronization, 1 PPS pulse from the GNSS receiver should be used to synchronize the other sensors. Alternatively, precise quartz clocks such as TCXO or OCXO could be used for time synchronization. It should also be noted that the internal built-in RTC clocks have a drift and cannot be used for this type of synchronization at the level of 1  $\mu$ s.

## Funding

The research is co-financed under the Leading Research Groups support project from the subsidy increased for the period 2020–2025 in the amount of 2% of the subsidy referred to Art. 387 (3) of the Law of 20 July 2018 on Higher Education and Science, obtained in 2019, and a

project “Testing and optimizing the platform performance for precise positioning” grant no. Z030/0025/20 (B090/0052/19).

#### CRediT authorship contribution statement

**Adrian Kaczmarek:** Methodology, Validation, Formal analysis, Investigation, Visualization, Writing – original draft, Writing – review & editing. **Witold Rohm:** Methodology, Writing – original draft, Writing – review & editing, Supervision, Funding acquisition. **Lasse Klingbeil:** Methodology. **Janusz Tchorzewski:** Writing – original draft.

#### Declaration of Competing Interest

The authors declare that they have no known competing financial interests or personal relationships that could have appeared to influence the work reported in this paper.

#### References

- [1] A. Aboseeken, A. Noureldin, M.J. Korenberg, Improving the RISS/GNSS land-vehicles integrated navigation system using magnetic azimuth updates, *IEEE Trans. Intelligent Transportation Syst.* 21 (3) (2020) 1250–1263.
- [2] J. Bijkor, W. Steyn, Kalman filter configurations for a low-cost loosely integrated inertial navigation system on an airship, *Control Eng. Pract.* 16 (12) (2008) 1509–1518, <https://doi.org/10.1016/j.conengprac.2008.04.011>.
- [3] X. Chen, W. Hu, L. Zhang, Z. Shi, M. Li, Integration of low-cost GNSS and monocular cameras for simultaneous localization and mapping, *Sensors (Switzerland)* 18 (7) (2018) 2193, <https://doi.org/10.3390/s18072193>.
- [4] Chu, T., & Akos, D. (2011). Assisted GNSS - Performance Results of Multiplexed Measurements, Limited Bandwidth, and a Vectorized Implementation. *Proceedings of the 2011 International Technical Meeting of The Institute of Navigation*, 1007–1018.
- [5] T. Chu, N. Guo, S. Backén, D. Akos, Monocular Camera/IMU/GNSS Integration for Ground Vehicle Navigation in Challenging GNSS Environments, *Sensors* 12 (3) (2012) 3162–3185, <https://doi.org/10.3390/s120303162>.
- [6] M. Dorn, R. Lesjak, M. Wieser, Improvement of the standard GNSS/IMU solution for UAVs using already existing redundant navigation sensors. *European Navigation Conference ENC 2016*, 2016, 10.1109/EURONAV.2016.7530567.
- [7] Elisson, V., & Assler, G. G. (2014). *Low cost relative GNSS positioning with IMU integration*. <https://odr.chalmers.se/bitstream/20.500.12380/200466/1/200466.pdf>. Data accessed: 16.06.2021.
- [8] M. Elsheikh, A. Noureldin, M. Korenberg, Integration of GNSS Precise Point Positioning and Reduced Inertial Sensor System for Lane-Level Car Navigation, *IEEE Trans. Intell. Transp. Syst.* 1–16 (2020), <https://doi.org/10.1109/TITS.2020.3040955>.
- [9] S. Gan-Mor, R.L. Clark, B.L. Upchurch, Implement lateral position accuracy under RTK-GPS tractor guidance, *Comput. Electron. Agric.* 59 (1–2) (2007) 31–38.
- [10] S. Godha, M.E. Cannon, GPS/MEMS INS integrated system for navigation in urban areas, *GPS Solutions* 11 (3) (2007) 193–203, <https://doi.org/10.1007/s10291-006-0050-8>.
- [11] M.S. Grewal, A.P. Andrews, C.G. Bartone (Eds.), *Global Navigation Satellite Systems, Inertial Navigation, and Integration*, Wiley, 2020.
- [12] J.-H. Han, C.-h. Park, C.-K. Hong, J.H. Kwon, Performance Analysis of Two-Dimensional Dead Reckoning Based on Vehicle Dynamic Sensors during GNSS Outages, *J. Sens.* 2017 (2017) 1–13.
- [13] J.-H. Han, C.-h. Park, Y.-J. Park, J.H. Kwon, Preliminary Results of the Development of a Single-Frequency GNSS RTK-Based Autonomous Driving System for a Speed Sprayer, *J. Sens.* 2019 (2019) 1–9.
- [14] B. Hofmann-Wellenhof, H. Lichtenegger, E. Wasle, *GNSS-global navigation satellite systems: GPS, GLONASS, Galileo, and more*, Springer, 2007.
- [15] Langley, R. B. (1998). *RTK GPS*. <http://www2.unb.ca/gge/Resources/gpsworld/september98.pdf> - accessed 11.01.2022. Date accessed: 11.01.2022.
- [16] L. Lasmadi, A. Cahyadi, S. Herdjunkanto, R. Hidayat, Inertial navigation for quadrotor using kalman filter with drift compensation, *Int. J. Electrical Comput. Eng.* 7 (5) (2017) 2596–2604, <https://doi.org/10.11591/ijece.v7i5.pp2596-2604>.
- [17] T. Li, H. Zhang, Z. Gao, X. Niu, N. El-sheimy, Tight Fusion of a Monocular Camera, MEMS-IMU, and Single-Frequency Multi-GNSS RTK for Precise Navigation in GNSS-Challenged Environments, *Remote Sens.* 11 (6) (2019) 610, <https://doi.org/10.3390/rs11060610>.
- [18] Y. Li, A. Dempster, B. Li, J. Wang, C. Rizos, A Low-cost Attitude Heading Reference System by Combination of GPS and Magnetometers and MEMS Inertial Sensors for Mobile Applications, *J. Global Position. Syst.* 5 (1&2) (2006) 88–95, <https://doi.org/10.5081/jgps.5.1.88>.
- [19] K.Q. Lin, Z.L. Deng, L. Yin, Effective multipath mitigation methods for RTK in urban environments, *Lecture Notes Electrical Eng.* 499 (2018) 565–576, [https://doi.org/10.1007/978-981-13-0029-5\\_49](https://doi.org/10.1007/978-981-13-0029-5_49).
- [20] Madgwick, S. (2010). An efficient orientation filter for inertial and inertial/magnetic sensor arrays. In *forums.parallax.com*. <https://forums.parallax.com/uploads/attachments/41167/106661.pdf>. Date accessed: 16.06.2021.
- [21] R. Mahony, T. Hamel, J.-M. Pflemlin, *Complementary Filters on the Special Orthogonal Group*, in: *IEEE Transactions on Automatic Control*, Institute of Electrical and Electronics Engineers, 2008, pp. 1203–1217, 10.1109/TAC.2008.923738i.
- [22] Mongréden, C., Doyen, J. P., Ström, M., & Ammann, D. (2016). Centimeter-Level Positioning for UAVs and Other Mass-Market Applications. *29th International Technical Meeting of the Satellite Division of the Institute of Navigation, ION GNSS 2016*, 2, 1441–1454. <https://doi.org/10.33012/2016.14619>.
- [23] Z. Nie, F. Liu, Y. Gao, Real-time precise point positioning with a low-cost dual-frequency GNSS device, *GPS Solutions* 24 (1) (2020), <https://doi.org/10.1007/S10291-019-0922-3>.
- [24] N. Noguchi, J.F. Reid, Q. Zhang, J.D. Will, K. Ishii, et al., Development of robot tractor based on RTK-GPS and gyroscope, in: 2001 ASAE Annual Meeting, 1998, p. 1.
- [25] M. O'Connor, T. Bell, G. Elkaim, B. Parkinson, Automatic steering of farm vehicles using GPS, in: *Proceedings of the Third International Conference on Precision Agriculture*, 1996, pp. 767–777.
- [26] R. Odolinski, P. Teunissen, Single-frequency, dual-GNSS versus dual-frequency, single-GNSS: a low-cost and high-grade receivers GPS-BDS RTK analysis, *J. Geod.* 90 (11) (2016) 1255–1278, <https://doi.org/10.1007/S00190-016-0921-X>/TABLES/18.
- [27] R. Odolinski, P. Teunissen, Best integer equivariant estimation: performance analysis using real data collected by low-cost, single- and dual-frequency, multi-GNSS receivers for short- to long-baseline RTK positioning, *J. Geod.* 94 (9) (2020), <https://doi.org/10.1007/S00190-020-01423-2>.
- [28] C. Park, J. Han, Performance Evaluation of GNSS and Motion Sensor Integrated Positioning Algorithm for Land Vehicle Monitoring, in: *2020 International Conference on Information and Communication Technology Convergence (ICTC)*, 2020, pp. 1592–1595.
- [29] M. Park, Y. Gao, Error and Performance Analysis of MEMS-based Inertial Sensors with a Low-cost GPS Receiver, *Sensors* 8 (4) (2008) 2240–2261.
- [30] E.B. Quist, R.W. Beard, Radar odometry on small unmanned aircraft, in: *AIAA Guidance, Navigation, and Control (GNC) Conference*, 2013, <https://doi.org/10.2514/6.2013-4698>.
- [31] Sheng, H. L., Zhang, T. H., & Liu, D. D., 2013. Low-cost AHRS design based on extending Kalman filter. *Xi Tong Gong Cheng Yu Dian Zi Ji Shu/Systems Engineering and Electronics*, 35(10), 2158–2164. <https://doi.org/10.3969/j.issn.1001-506X.2013.10.23>.
- [32] Shin, E. (2001). Accuracy improvement of low cost INS/GPS for land applications [University of Calgary]. In *ion.org*. <https://doi.org/10.11575/PRISM/23262>.
- [33] J. Simanek, M. Reinstein, V. Kubelka, Evaluation of the EKF-based estimation architectures for data fusion in mobile robots, *IEEE/ASME Trans. Mechatron.* 20 (2) (2015) 985–990, <https://doi.org/10.1109/TMECH.2014.2311416>.
- [34] A. Stoll, H. Kutzbach, Guidance of a forage harvester with GPS, *Precis. Agric.* 2 (3) (2000) 281–291.
- [35] P. Strode, P. Groves, GNSS multipath detection using three-frequency signal-to-noise measurements, *GPS Solutions* 20 (3) (2016) 399–412, <https://doi.org/10.1007/S10291-015-0449-1>/FIGURES/17.
- [36] R. Takai, L. Yang, N. Noguchi, Development of a crawler-type robot tractor using RTK-GPS and IMU, *Eng. Agric. Environ. Food* 7 (4) (2014) 143–147.
- [37] Tokura, H., & Kubo, N., 2016. Effective satellite selection methods for RTK-GNSS NLOS exclusion in dense urban environments. *29th International Technical Meeting of the Satellite Division of the Institute of Navigation, ION GNSS 2016*, 1, 304–312. <https://doi.org/10.33012/2016.14801>.
- [38] u-blox, 2017. NEO-M8P u-blox M8 high precision GNSS modules Data sheet Title NEO-M8P Subtitle u-blox M8 high precision GNSS modules Document type Data sheet Document number This document applies to the following products: Product name Type number ROM/FLASH version PC.
- [39] u-blox, 2020a. NEO-M8P u-blox M8 high precision GNSS modules Data sheet Document information Title NEO-M8P Subtitle u-blox M8 high precision GNSS modules Document type Data sheet Document number This document applies to the following products: Product name Type number R.
- [40] u-blox, 2020b. NEO/LEA-M8T u-blox M8 concurrent GNSS timing modules Data sheet Document information Title NEO/LEA-M8T Subtitle u-blox M8 concurrent GNSS timing modules Document type Data sheet Document number This document applies to the following products: Product name Type number ROM/FLASH version PCN reference.
- [41] J. Wang, M. Garratt, A. Lambert, J. Wang, S. Han, D. Sinclair, Integration of GPS/INS/vision sensors to navigate unmanned aerial vehicles, *Int. Arch. Photogrammetry Remote Sens. Spatial Info. Sci.* 37 (2008) 963–970.
- [42] D.H. Won, E. Lee, M. Heo, S. Sung, J. Lee, Y.J. Lee, GNSS integration with vision-based navigation for low GNSS visibility conditions, *GPS Solutions* 18 (2) (2014) 177–187, <https://doi.org/10.1007/s10291-013-0318-8>.
- [43] Xia, G., Wang, G., Chen, X., & Xue, J. (2016). Low-cost MEMS-INS/GNSS integration using quaternion-based nonlinear filtering methods for USV. *OCEANS 2016 - Shanghai*. <https://doi.org/10.1109/OCEANSAP.2016.7485595>.
- [44] X. Yin, J. Du, D. Geng, C. Jin, Development of an automatically guided rice transplanter using RTK-GNSS and IMU, *IFAC-PapersOnLine* 51 (17) (2018) 374–378.

- [45] xsens, 2021. *MTi user manual and technical documentation - Google Scholar*. [https://www.xsens.com/hubfs/Downloads/usermanual/MTi\\_usermanual.pdf](https://www.xsens.com/hubfs/Downloads/usermanual/MTi_usermanual.pdf). Date accessed: 16.06.2021.
- [46] Q. Zhou, H. Zhang, Y. Li, Z. Li, An Adaptive Low-Cost GNSS/MEMS-IMU Tightly-Coupled Integration System with Aiding Measurement in a GNSS Signal-Challenged Environment, Sensors 15 (2015) 23953–23982, <https://doi.org/10.3390/s150923953>.
- [47] Z. Zhu, C. Jiang, Y. Bo, Performance Enhancement of GNSS/MEMS-IMU Tightly Integration Navigation System Using Multiple Receivers, IEEE Access 8 (2020) 52941–52949, <https://doi.org/10.1109/ACCESS.2020.2981769>.